Accelerated Boundary Element Modeling of Lossy Conductors in Layered Media with a Single-Source Surface Impedance Operator

Shashwat Sharma, Piero Triverio
Department of Electrical & Computer Engineering, University of Toronto, Canada
shash.sharma@mail.utoronto.ca, piero.triverio@utoronto.ca

***Abstract*—A new boundary element formulation is presented for the electromagnetic analysis of interconnects in layered media, which accurately captures skin effect in conductors of arbitrary shape and size. Results show superior CPU-time and memory performance compared to several state-of-the-art techniques.**

***Index Terms*—Surface integral equations, layered media, lossy conductors**

I. Introduction

The accurate electromagnetic modeling of skin effect over a broad frequency range is essential in the design of integrated circuits, for the quantification of signal integrity phenomena in high-speed on-chip interconnects. Volume-based numerical methods, such as the finite element method (FEM) [1] or volume integral equations [2], require an extremely fine volumetric mesh for the structure to resolve the small skin depth at high frequencies, which is expensive. The boundary element method (BEM) is an appealing alternative, since it requires only a surface-based discretization of the objects in the structure [3].

Conductor modeling with the BEM requires formulating an interior problem to capture the skin effect inside objects, and an exterior problem to model coupling between them. The generalized impedance boundary condition (GIBC) [4] is an accurate and well-conditioned formulation for skin effect modeling, but requires both single- and double-layer potential operators [3] for the exterior problem. The computation of both operators is expensive for objects embedded in layered media, since the expensive multilayer Green's function and its curl are both required [5]. Multi-region formulations like [6] suffer from the same drawback, and also require expensive dual basis functions to achieve good conditioning [7].

A single-layer impedance matrix (SLIM) formulation was recently proposed [8]. The SLIM method is formulated in terms of a single source [9] and does not require the double-layer potential operator for the exterior problem, and therefore avoids the computational and implementation costs associated with the curl of the MGF. Unlike preceding single-source formulations [10], the SLIM method is well conditioned even without dual basis functions [8]. However, the SLIM approach requires factorizing two dense matrices per object, which is only feasible for small objects.

In this work, an accelerated SLIM formulation is proposed, which avoids the assembly and factorization of dense matrices in the interior problem and allows handling large objects efficiently. This is achieved with the use of an object-wise adaptive integral method (AIM) [11] to accelerate matrix-vector products associated to the interior problem [12].

This work was supported by the Natural Sciences and Engineering Research Council of Canada, by Advanced Micro Devices, and by CMC Microsystems.

978-1-7281-6161-7/20/$31.00 ©2020 IEEE

II. Proposed Formulation

We consider a homogeneous object bounded by a surface $\mathcal{S}$ with outward unit normal vector $\hat{n}$. The object has permittivity ε', conductivity σ, and $\varepsilon \triangleq \varepsilon' - j\sigma/\omega$, where ω is the cyclical frequency. A triangular mesh is generated for $\mathcal{S}$. The object is embedded in a layered medium, where the l^{th} layer has permittivity ε_l and permeability μ_l.

A. Interior Problem

1) Original Configuration: The tangential electric and magnetic fields on $\mathcal{S}$ are related via the magnetic field integral equation (MFIE) [3], which is discretized and tested using RWG and $\hat{n} \times$ RWG basis functions [3], respectively, to get

$$-j\omega\varepsilon\,\mathbf{L}\mathbf{E} - \left(\mathbf{K} - \frac{1}{2}\mathbf{I}_{\times}\right)\mathbf{H} = \mathbf{0}, \tag{1}$$

where the entries of matrices $\mathbf{L}$ and $\mathbf{K}$ may be found in literature [3], and involve the homogeneous Green's function of the object's material. Matrix $\mathbf{I}_{\times}$ is the identity operator obtained when RWG functions are tested with $\hat{n} \times$ RWG functions. Column vectors $\mathbf{E}$ and $\mathbf{H}$ contain the coefficients of the basis functions associated with the tangential electric and magnetic fields, respectively. Vector $\mathbf{E}$ can be expressed in terms of $\mathbf{H}$ with a rearrangement of (1),

$$\mathbf{E} = \frac{-1}{j\omega\varepsilon}\left(\mathbf{L}\right)^{-1}\left(\mathbf{K} - \frac{1}{2}\mathbf{I}_{\times}\right)\mathbf{H} = \mathbf{Z}\mathbf{H}, \tag{2}$$

where $\mathbf{Z}$ may be interpreted as the surface impedance operator associated to the object [4].

2) Equivalent Configuration: Next, we use the surface equivalence principle to replace the conductive object with the background material in which it resides, while requiring that the tangential electric field remains unchanged for $\vec{r} \in \mathcal{S}$ [9]. An equivalent electric current density, $\mathbf{J}_{\Delta} = \mathbf{H} - \mathbf{H}_{\text{eq}}$, must

be introduced on $\mathcal{S}$ to keep fields exterior to $\mathcal{S}$ unchanged, where $\mathbf{H}_{\rm eq}$ is the discretized tangential magnetic field on $\mathcal{S}$ in the equivalent configuration.

In the equivalent configuration, the fields tangental to $\mathcal{S}$ can also be related via the discretized electric field integral equation (EFIE) [3]

$$j\omega\mu_l \, \mathbf{L}_l \mathbf{H}_{\rm eq} - \left(\mathbf{K}_l - \frac{1}{2}\mathbf{I}_\times \right) \mathbf{E} = \mathbf{0}, \tag{3}$$

where $\mathbf{L}_l$ and $\mathbf{K}_l$ involve the homogeneous Green's function of the medium just outside $\mathcal{S}$. The equivalent tangential magnetic field $\mathbf{H}_{\rm eq}$ may be expressed in terms of $\mathbf{E}$ with a rearrangement of (3),

$$\mathbf{H}_{\rm eq} = \frac{1}{j\omega\mu_{\rm eq}} \left(\mathbf{L}_{\rm eq}\right)^{-1} \left(\mathbf{K}_{\rm eq} - \frac{1}{2}\mathbf{I}_{\rm x} \right) \mathbf{E} = \mathbf{Y}_{\rm eq}\mathbf{E}. \tag{4}$$

where $\mathbf{Y}_{\rm eq}$ may be interpreted as the surface admittance operator of the object filled with the surrounding medium [10].

B. Exterior Problem

The augmented EFIE (AEFIE) [13] is employed to model the exterior problem over a broad frequency range. The discretized charge density $\boldsymbol{\rho}_\Delta$ associated to $\mathbf{J}_\Delta$ is introduced as an additional unknown [13] to yield

$$jk_0\mathbf{L}_{\rm m}^{(A)}\mathbf{J}_\Delta + c_0\mathbf{D}^T\mathbf{L}_{\rm m}^{(\phi)}\mathbf{B}\boldsymbol{\rho}_\Delta + \eta_0^{-1}\mathbf{I}_\times\mathbf{E} = \eta_0^{-1}\mathbf{E}_{\rm inc}, \tag{5}$$

where $\mathbf{L}_{\rm m}^{(A)}$ and $\mathbf{L}_{\rm m}^{(\phi)}$ are, respectively, the discretized vector and scalar potential parts of the single-layer operator for the exterior problem, and involve the MGF. Column vector $\mathbf{E}_{\rm inc}$ is related to the incident electric field. Quantities k_0, η_0, and c_0 are, respectively, the wave number, wave impedance, and speed of light in free space. Definitions of the sparse matrices $\mathbf{D}$ and $\mathbf{B}$ may be found in [13].

Equations (2), (4) and the definition of $\mathbf{J}_\Delta$ are then used in (5) to obtain the final system of equations

$$\begin{bmatrix} jk_0\mathbf{L}_{\rm m}^{(A)} + \mathbf{C} & \mathbf{D}^T\mathbf{L}_{\rm m}^{(\phi)}\mathbf{B} \\ \mathbf{F}\mathbf{D}\left(\mathbf{I} - \mathbf{Y}_{\rm eq}\mathbf{Z}\right) & jk_0\mathbf{I} \end{bmatrix} \begin{bmatrix} \mathbf{H} \\ c_0\boldsymbol{\rho}_\Delta \end{bmatrix} = \begin{bmatrix} \mathbf{E}_{\rm inc}/\eta_0 \\ \mathbf{0} \end{bmatrix}, \tag{6}$$

where $\mathbf{C} = \left(-jk_0\mathbf{L}_{\rm m}^{(A)}\mathbf{Y}_{\rm eq} + \frac{1}{\eta_0}\mathbf{I}_\times \right)\mathbf{Z}$. The second row of (6) is the discretized continuity equation relating $\mathbf{J}_\Delta$ and $\boldsymbol{\rho}_\Delta$ [13]. Matrix $\mathbf{F}$ is defined in [13], and $\mathbf{I}$ is the identity matrix. Equation (6) is the SLIM formulation [8], which is well-conditioned and avoids the double-layer potential operator for the exterior problem, unlike the GIBC [4]. To solve (6) iteratively, the matrix-vector products involving $\mathbf{L}_{\rm m}^{(A)}$ and $\mathbf{L}_{\rm m}^{(\phi)}$ are accelerated with a multilayer AIM [14].

C. Accelerated Modeling of the Interior Problem

Solving (6) iteratively requires computing the two following matrix-vector products at each iteration k:

$$\mathbf{a}^{(k)} = \mathbf{Z}\mathbf{H}^{(k)} = \left(\frac{-\left(\mathbf{L}\right)^{-1}}{j\omega\varepsilon} \left(\mathbf{K} - \frac{1}{2}\mathbf{I}_\times \right) \right) \mathbf{H}^{(k)}, \tag{7}$$

$$\mathbf{b}^{(k)} = \mathbf{Y}_{\rm eq}\mathbf{a}^{(k)} = \left(\frac{\left(\mathbf{L}_{\rm eq}\right)^{-1}}{j\omega\mu_{\rm eq}} \left(\mathbf{K}_{\rm eq} - \frac{1}{2}\mathbf{I}_{\rm x} \right) \right) \mathbf{a}^{(k)}. \tag{8}$$

For large objects, the matrix inversions in (7) and (8) are not feasible. Instead, with a rearrangement of the matrices to be inverted, (7) and (8) are rewritten as two systems of equations,

$$\mathbf{L}\mathbf{a}^{(k)} = \frac{-1}{j\omega\varepsilon} \left(\mathbf{K} - \frac{1}{2}\mathbf{I}_\times \right) \mathbf{H}^{(k)}, \tag{9}$$

$$\mathbf{L}_{\rm eq}\mathbf{b}^{(k)} = \frac{1}{j\omega\mu_{\rm eq}} \left(\mathbf{K}_{\rm eq} - \frac{1}{2}\mathbf{I}_{\rm x} \right) \mathbf{a}^{(k)}. \tag{10}$$

Since systems (9) and (10) are "nested" into (6), their solution must be computed at every iteration k, and can seriously burden CPU time. To avoid this bottleneck, we propose an efficient preconditioning and solution strategy for (9) and (10). The AIM is used to accelerate all matrix-vector products involving $\mathbf{L}$, $\mathbf{K}$, $\mathbf{L}_{\rm eq}$ and $\mathbf{K}_{\rm eq}$. An independent AIM grid is generated for each object [12]. We can write $\mathbf{A} \approx \mathbf{A}_{\rm NR} + \mathbf{A}_{\rm FR}$, where $\mathbf{A} \in \{\mathbf{L}, \mathbf{K}, \mathbf{L}_{\rm eq}, \mathbf{K}_{\rm eq}\}$, $\mathbf{A}_{\rm NR}$ is sparse and contains the near-region entries of $\mathbf{A}$ which have been pre-corrected to account for the AIM grid contributions [15], and $\mathbf{A}_{\rm FR}$ contains far-region interactions. Matrix-vector products involving $\mathbf{A}_{\rm FR}$ are computed with the fast Fourier transform (FFT) [15]. The near-region entries of $\mathbf{L}$ and $\mathbf{L}_{\rm eq}$ are used as preconditioners for the efficient solution of (9) and (10), respectively. The proposed acceleration scheme allows the SLIM method to capture all electromagnetic phenomena inside conductors, both small and large, in an efficient, accurate and broadband way.

III. Results

We consider two examples: an on-chip inductor coil [15], and a portion of an interposer with 80 copper signal lines and a finite ground plane (courtesy of Dr. Rubaiyat Islam, Advanced Micro Devices). Both structures are embedded in a dielectric substrate ($\varepsilon_r = 2.1$ and 4, respectively) backed by a silicon layer over an infinite ground plane. The geometry and electric surface current densities are shown for the inductor and the interposer in the top panels of Fig. 1 and Fig. 2, respectively. For the inductor, the proposed method is compared against the DSA [10], GIBC [4] and SLIM [8] formulations, which all require the factorization of dense matrices for the interior problem. Results are also compared against a commercial finite element solver, Ansys HFSS. The scattering (S) parameters in Fig. 1 confirm the accuracy of the proposed method. Table I shows that the proposed method is between 1.5 and $16\times$ faster than all other methods, and among the most memory efficient. The SLIM formulation also requires, on average, $31\times$ fewer iterations than the DSA method. For the interposer, the proposed method is compared to HFSS, and to a recently-proposed accelerated GIBC formulation [12], where matrix factorizations in the interior problem are avoided. A comparison against DSA [10] and GIBC [4] was not feasible within the available $256\,$GB of memory. Similarly, HFSS was not able to accurately resolve skin effect beyond about $30\,$GHz without running out of memory, so a coarser mesh had to be used. The coarse HFSS mesh has 2–4 volume elements spanning the conductor cross section, while the skin depth becomes over $10\times$ smaller than the cross sectional dimensions. The S parameters reported in the bottom panel of Fig. 2

TABLE I: Performance comparison for the examples in Section III, on a 3 GHz Intel Xeon CPU, single-threaded.

	Inductor (4,470 triangles, 22 frequency points)					Interposer (156,820 triangles, 31 frequency points)			
	HFSS	DSA [10]	GIBC [4]	SLIM [8]	Proposed	HFSS	HFSS (coarse)	Accel. GIBC [12]	Proposed
Total CPU time (hours)	2.5	10.2	1.0	4.1	0.6	N/A	41.0	212.1	104.4
Peak memory (GB)	16.7	7.2	1.0	6.8	1.2	> 256	189.2	30.5	28.3

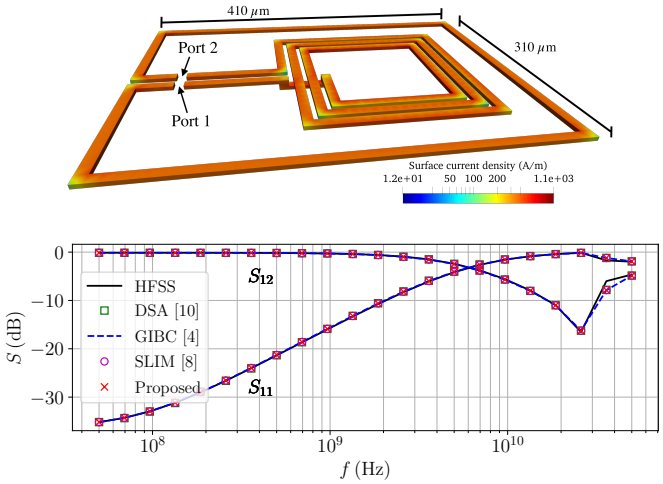

Fig. 1: Top panel: geometry of the inductor in Section III, with the electric surface current density at 100 MHz. Bottom panel: comparison of scattering parameters.

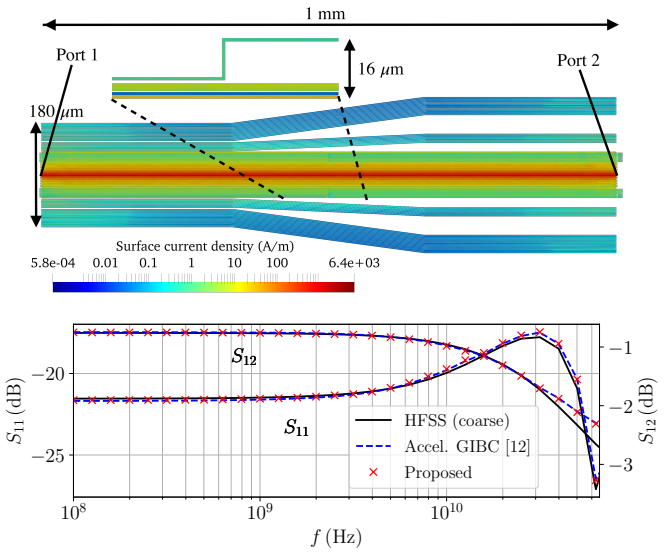

Fig. 2: Top panel: geometry of the interconnect network in Section III, with the electric surface current density at 1 GHz. Bottom panel: comparison of scattering parameters.

show an excellent match between the two BEM approaches. Results are also in agreement with HFSS up to about 30 GHz. Beyond this frequency, HFSS results start deviating due to the shrinking skin depth. Table I confirms that the proposed method is faster than the accelerated GIBC by a factor of over $2\times$, since the double-layer potential is avoided in the exterior problem. The proposed method is also $6.7\times$ more memory efficient than HFSS with the coarse mesh, while providing better accuracy beyond 30 GHz. In conclusion, the numerical examples considered demonstrate that the proposed method can efficiently model large realistic lossy conductors in layered media, thanks to an object-wise application of the AIM, and is significantly more efficient than representative BEM and FEM techniques from the state of the art.

References

[1] J.-M. Jin, *The Finite Element Method in Electromagnetics*, 3rd ed. Hoboken, NJ, USA: Wiley, 2014.

[2] A. E. Ruehli, G. Antonini, and L. Jiang, *Circuit Oriented Electromagnetic Modeling Using the PEEC Techniques*. IEEE Press, 2017.

[3] W. C. Gibson, *The Method of Moments in Electromagnetics*. Boca Raton, FL, USA: CRC press, 2014.

[4] Z. G. Qian, W. C. Chew, and R. Suaya, "Generalized impedance boundary condition for conductor modeling in surface integral equation," *IEEE Trans. Microw. Theory Tech.*, vol. 55, no. 11, pp. 2354–2364, Nov. 2007.

[5] K. A. Michalski and J. R. Mosig, "Multilayered media Green's functions in integral equation formulations," *IEEE Trans. Antennas Propag.*, vol. 45, no. 3, pp. 508–519, Mar. 1997.

[6] T. Xia, H. Gan, M. Wei, W. C. Chew, H. Braunisch, Z. Qian, K. Aygün, and A. Aydiner, "An integral equation modeling of lossy conductors with the enhanced augmented electric field integral equation," *IEEE Trans. Antennas Propag.*, vol. 65, no. 8, pp. 4181–4190, Aug. 2017.

[7] A. Buffa and S. H. Christiansen, "A dual finite element complex on the barycentric refinement," *Math. Computation*, vol. 76, pp. 1743–1769, 2007.

[8] S. Sharma and P. Triverio, "SLIM: A well-conditioned single-source boundary element method for modeling lossy conductors in layered media," *IEEE Antennas Wireless Propag. Lett.*, 2020 (accepted, axXiv: 2007.07378).

[9] M. Huynen, K. Y. Kapusuz, X. Sun, G. Van der Plas, E. Beyne, D. De Zutter, and D. Vande Ginste, "Entire domain basis function expansion of the differential surface admittance for efficient broadband characterization of lossy interconnects," *IEEE Trans. Microw. Theory Tech.*, vol. 68, no. 4, pp. 1217–1233, Jan. 2020.

[10] U. R. Patel, S. Sharma, S. Yang, S. V. Hum, and P. Triverio, "Full-wave electromagnetic characterization of 3D interconnects using a surface integral formulation," in *IEEE EPEPS*, San Jose, CA, Oct. 2017.

[11] E. Bleszynski, M. Bleszynski, and T. Jaroszewicz, "AIM: Adaptive integral method for solving large-scale electromagnetic scattering and radiation problems," *Radio Sci.*, vol. 31, no. 5, pp. 1225–1251, Sep. 1996.

[12] S. Sharma and P. Triverio, "A fully-accelerated surface integral equation method for the electromagnetic modeling of arbitrary objects," *IEEE Trans. Antennas Propag.*, 2020 (submitted, arXiv: 2003.11679).

[13] Z.-G. Qian and W. C. Chew, "Fast full-wave surface integral equation solver for multiscale structure modeling," *IEEE Trans. Antennas Propag.*, vol. 57, no. 11, pp. 3594–3601, Nov. 2009.

[14] S. Sharma, U. R. Patel, S. V. Hum, and P. Triverio, "A complete surface integral method for broadband modeling of 3D interconnects in stratified media," *arXiv e-prints*, p. arXiv: 1810.04030, Oct. 2018.

[15] T. Moselhy, X. Hu, and L. Daniel, "pFFT in FastMaxwell: A fast impedance extraction solver for 3D conductor structures over substrate," in *Proc. Conf. Des., Automat. Test*, 2007.